

Non-linear optimized spatial filter for single-trial identification of movement related cortical potential

Original

Non-linear optimized spatial filter for single-trial identification of movement related cortical potential / Mascolini, A.; Niazi, I. K.; Mesin, L.. - In: BIOCYBERNETICS AND BIOMEDICAL ENGINEERING. - ISSN 0208-5216. - 42:1(2022), pp. 426-436. [10.1016/j.bbe.2022.02.013]

Availability:

This version is available at: 11583/2959492 since: 2022-03-28T15:01:28Z

Publisher:

Elsevier B.V.

Published

DOI:10.1016/j.bbe.2022.02.013

Terms of use:

This article is made available under terms and conditions as specified in the corresponding bibliographic description in the repository

Publisher copyright

Elsevier postprint/Author's Accepted Manuscript

© 2022. This manuscript version is made available under the CC-BY-NC-ND 4.0 license
<http://creativecommons.org/licenses/by-nc-nd/4.0/>. The final authenticated version is available online at:
<http://dx.doi.org/10.1016/j.bbe.2022.02.013>

(Article begins on next page)

Non-linear Optimized Spatial Filter for Single-Trial Identification of Movement Related Cortical Potential

Abstract

To investigate the optimal filter settings for pre-processing of Movement Related Cortical Potentials (MRCP) for the detection through EEG in single trial, we have proposed a novel Non-Linear Optimized Spatial Filter (NL-SF) and compared it to the Optimized Spatial Filtering (OSF) used in literature. MRCPs from EEG recordings are emphasized, calculating the optimal non-linear combination of channels which isolates the signal of interest. The method is applied to EEG data recorded from 16 healthy patients either executing or imagining 50 self-paced upper limb movements (palmar grasp). MRCPs have been identified from the outputs of the two filters by matching with a template built by averaging responses to movement intentions in the training set. NL-SF had a median accuracy on the overall dataset of 84.6%, which is significantly better than that of OSF (i.e., 76.9%). Being a filter and feasible for self-paced applications, it could be of interest in online BCI system design.

Keywords: Surface EEG, Brain computer interface, Spatial filters

1. Introduction

2 The Movement Related Cortical Potential (MRCP) is a low frequency negative
3 shift in the EEG signal appearing around 2 seconds before a planned or executed
4 voluntary movement [1][2]. Its detection can be instrumental in the development
5 of Brain Computer Interfaces (BCI) which allow communication of patients who
6 are otherwise unable, as well as in the neurorehabilitation of people with motor
7 impairments [3]. An improvement in accuracy of the detectors could lead to a
8 significant advancement in the field of neuroprosthetics [4].

9 BCIs are a relatively recent subject of research, with the first paper on the topic
10 published in 1973 [5]. The term BCI encompasses multiple types of techniques
11 to allow machine-brain communication, which are helpful for patients with con-
12 ditions which do not allow them to communicate with the external world, such
13 as locked-in syndrome [6], amyotrophic lateral sclerosis [7] and cerebral palsy [8].
14 This kind of assistive technology gives these patients the ability to communicate,
15 providing a significant improvement of their quality of life [9].

16 Nonetheless current BCIs have many challenges, such as providing precise biofeed-
17 back to the user: lack of touch, pressure, muscle lengthening and proprioception
18 render the feedback poorly effective [10]. Indeed, the subject can usually only
19 use sight to understand the difference between the desired action and the actual
20 BCI output. Another important issue is latency: if the delay between the action
21 and its feedback is too long, the ability of the patient to learn and improve the
22 effective control of the BCI can be severely affected [11].

23 Different approaches have been explored in the literature of BCI systems, e.g.,
24 event-related potentials like P300 [12], steady-state visual evoked potentials
25 (SSVEP, [13]), low frequency asynchronous switch design [14]. Here we focus
26 on the detector performance of MRCP [1][2] (see an example in Figure 1). This
27 EEG potential can be seen before a planned voluntary movement, both when
28 it is executed and when it is simply imagined [1]. Moreover, the MRCP is
29 found even if the patient is not physically capable of performing the movement,
30 rendering its detection a good candidate for a BCI application [15].

31 MRCPs have been studied for decades [1]. Research in the field has shown that
32 their size and delay are adjusted according to the participants' mental state
33 and characteristics of the executed movement, such as speed, accuracy and
34 frequency. Moreover, these potentials contain important information, including
35 the intended limb, grasp force, speed and direction of the movement [16].

36 Efforts have been devoted to developing systems for single trial MRCP detection
37 for application in BCIs [17]. These attempts have been hindered by what is

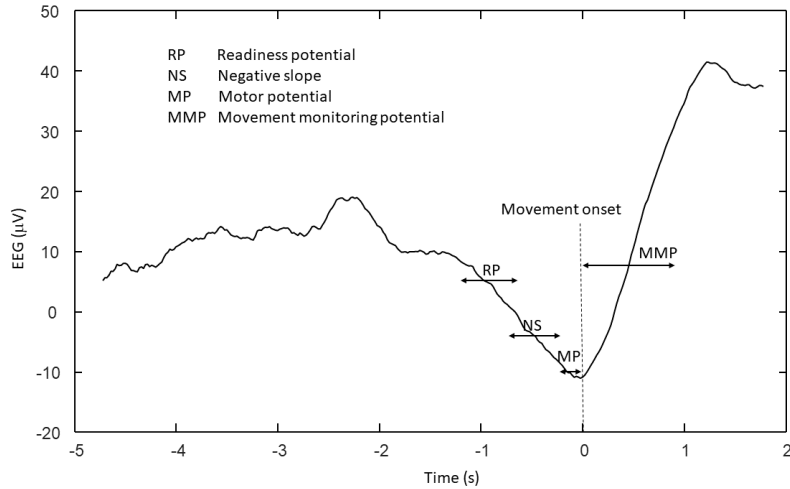


Figure 1: MRCPs of a healthy subject (participant number 1) in the case of motor execution. The wave was obtained by an average of 50 large Laplacian spatial filtered EEG trials.

38 a common issue in BCIs, i.e., the signal to noise ratio (SNR), which is very
 39 low (like most endogenous brain potentials recorded through the EEG). This
 40 reduces the accuracy of detection methods [18]. However, clinical studies have
 41 shown that participants can learn how to control and amplify MRCPs through
 42 training [19][20]. Individually calibrating endogenous BCIs has been postulated
 43 to be the solution to these problems [21]. Another important issue is the need
 44 of performing MRCP identification in order to give the user the impression to
 45 control the BCI in real-time [22].

46 In this paper, an innovative technique is proposed to identify the MRCP. It
 47 is based on the estimation of an optimal non-linear combination of channels
 48 which isolates the waveforms of interest and maps them on a prototype, thus
 49 imposing similar filter outputs during each movement intention. We expect
 50 that using a non-linear approach (instead of the usual linear one) and imposing
 51 similar output waveforms could result in better performance for the MRCP
 52 based detector compared to previously proposed methods.

53 **2. Materials and Methods**

54 In the following sections, the data collection will be outlined as well as the
55 analysis used in the current study.

56 *2.1. Experimental data*

57 *2.1.1. Subjects*

58 Sixteen healthy subjects aged 28 ± 12 years, 4 men and 12 women, with no his-
59 tory of neurological diseases, participated in the experiment. All subjects gave
60 their written informed consent. All procedures followed the tenets of the Dec-
61 laration of Helsinki and were approved by the local ethical committee (number
62 20130081).

63 *2.1.2. Experimental setup*

64 The subjects were placed in a chair in front of the computer with a hand force
65 transducer (Noraxon USA, Scottsdale, AZ) in the right hand. They performed
66 maximum voluntary contraction (MVC) three times and the highest value was
67 retained. Then, grasp trials were executed. A feedback was given to the partici-
68 pants to perform the grasp at 60% MVC force level during this motor execution
69 task. The force data was sampled at 2000 Hz. All participants performed 50
70 trials of both motor execution and motor imagination of palmer grasp. Each
71 movement type was performed 2×25 times with a 2-3-minute break after the
72 25th movement. The movements were performed in blocks; the order was ran-
73 domized. The subjects were visually cued (see Figure 2) by a custom-made
74 program (Aalborg University). The force produced during motor execution
75 tasks was recorded and used as input, so the subjects had continuous visual
76 feedback. During motor imagination tasks, a cursor moved over the template
77 (shown in Figure 2) to cue the subjects. Each trial had the following phases:
78 1) rest from -5 s to -3 s, 2) preparation for the task from -3 s to 0 s, 3) reach
79 60% MVC target level from 0 s to 0.5 s, 4) hold the contraction from 0.5 s to
80 1 s, 5) rest from 1 s to 3-5 s (thus, in total, the rest period varied between
81 5-7 seconds). For the tasks where the movements were executed, the force was

82 used to determine the movement onset. This was defined as the instant where
 83 all values in a 200-ms wide moving time window were above the baseline. The
 84 baseline was calculated from the recordings during the rest phase. All onsets
 were visually inspected.

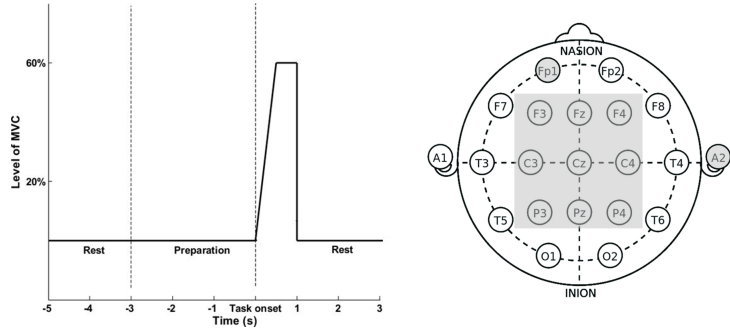


Figure 2: Left – visual cue provided to the participants. The entire template was visible from the beginning to the end of the trial. Subjects were asked to follow the template with the help of a moving cursor. For the Motor execution task, the output of the force transducer was used as a moving cursor, while, for motor imagination, the cursor moved over the template to cue the subjects. Right – EEG electrodes used in the study.

85

86 2.1.3. EEG Recording

87 Continuous 9 channel monopolar (Ag/AgCl ring electrodes) EEG (EEG Am-
 88 plifiers, Nuamps Express, Neuroscan) was recorded from the following channels
 89 (according to the International 10-20 system): F3, Fz, F4, C3, Cz, C4, P3, Pz
 90 and P4. The signals were referenced to the right ear lobe and grounded at na-
 91 sion. Electrooculography (EOG) was recorded from FP1. The EEG and EOG
 92 were sampled at 500 Hz and converted with 32-bit precision. The impedance of
 93 all electrodes was below 5 k Ω . During the recordings, the subjects were asked
 94 to minimize eye blinks and facial and body movements. A digital trigger was
 95 sent from the visual cueing program to the EEG amplifier at the beginning of
 96 each trial.

97 *2.2. Signal processing*

98 We have developed an innovative filter to improve the SNR of EEG recordings
99 containing MRCPs. The new method is compared to a state-of-the-art filter
100 proposed in the literature [2].

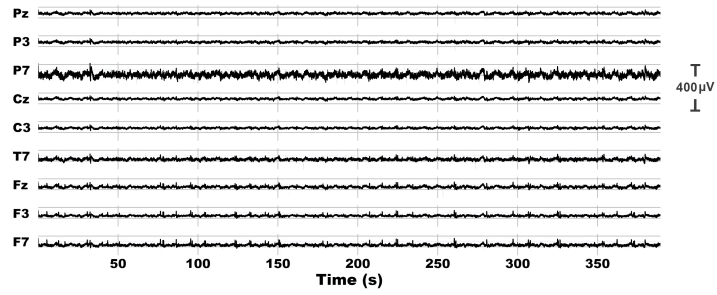
101 The data were divided as follows:

- 102 • All measurements from one participant (subject number 16) during motor
103 execution (50 trials) were devoted for hyper-parameter optimization;
- 104 • Every remaining session was divided in 2 parts, 70% for training and 30%
105 for testing.

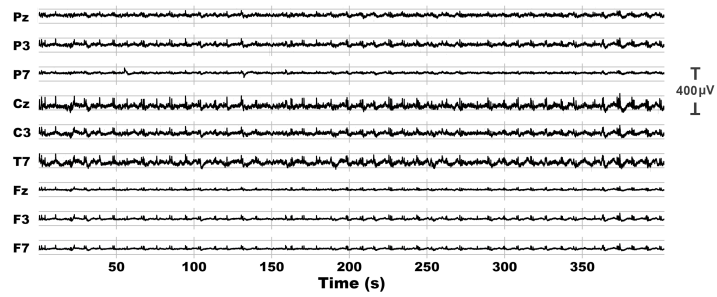
106 Every test set was consequent in time to the corresponding training set, as
107 to simulate a realistic calibration procedure. Some tests were also performed
108 considering a limited number of channels and a reduced training set.

109 The signals were high-pass filtered at 0.04 Hz, to remove low frequency drifts,
110 reflecting a measurement artifact (Butterworth filter with 40 dB per decade
111 of attenuation outside of the pass band) [2]. Blink artifacts exhibit a power
112 significantly higher than the rest of the signal, rendering filtering ineffective
113 as the low frequency components overlaying the MRCP are non-negligible [22].
114 Second Order Blind-source Identification (SOBI) [23] algorithm was shown to
115 be capable of reliably identifying and isolating blink artifacts [24]. Specifically,
116 the artifact was identified as included in the component (among those provided
117 by SOBI algorithm) with lowest fractal dimension (computed by the Sevcik's
118 method [25]). Such a component was removed before reconstructing the signal.
119 Some examples of filtered data to which blink artifacts have been removed are
120 shown in Figure 3.

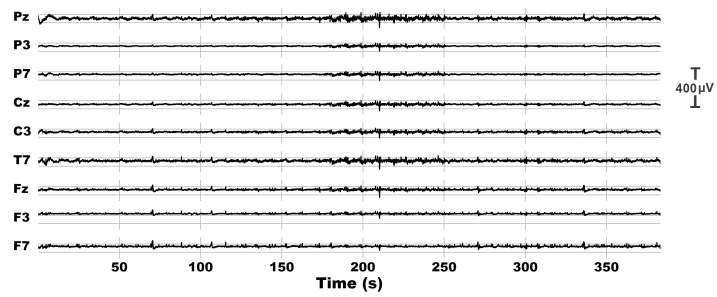
121 Some high frequency noise (e.g., due to EMG or electrical noise) was removed
122 by a low-pass filter. Specifically, a low-pass filter with cut-off 20 Hz was used
123 (Butterworth filter with roll-off 40 dB/decade). Moreover, the data were down-
124 sampled by a factor of 10, bringing the sampling frequency to 50 Hz.



(a) participant 1



(b) participant 2



(c) participant 3

Figure 3: Representative examples of portions of EEG data, after bandpass filtering and artifacts removal.

125 *2.3. Non-linear optimal spatial filter*

126 *2.3.1. Linear approach*

To introduce the problem, we discuss here the design of a linear filter, which is an approximation of the non-linear technique detailed in the following. The method strives to find the best weight vector W which, when multiplied by the EEG collected in the rows of matrix S , gives the best approximation of the MRCP component A of the signal

$$S \cdot W = A + \tau \tag{1}$$

127 where τ is a residual error, W is an unknown vector to be estimated (with
128 nc elements, where nc is the number of EEG channels), A is a time series
129 including a prototype of the MRCP (detailed below, with N_T samples, where
130 N_T is the number of time samples considered) and S is a matrix (of dimension
131 $nc \times N_T$) having in each row the EEG time series from a specific channel. This
132 linear model can be considered only as an approximation of the real situation.
133 Indeed, our ill-posed source separation problem could likely benefit from a non-
134 linear model. This observation suggested us to implement an algorithm able
135 to learn non-linear mappings (described in the following). This is despite most
136 authors managed the extraction of MRCPs from EEG recordings with fully
137 linear models, which are surely simpler to manage than non-linear ones.

138 Equation (1) is linear, in the canonical form of an Ordinary Least Squares (OLS)
139 problem. The OLS method allows to get the vector W which minimizes the
140 energy of the residual τ , under the following mathematical assumptions:

- 141 • residuals have zero conditional mean;
- 142 • predictors are linearly independent;
- 143 • residuals are spherical.

144 The validity of the above assumptions will be analyzed in the Appendix.

145 A calibration process is used to estimate A , i.e., the MRCP component included
146 in the signal. Assuming the vector W to be constant in time (which is reason-

147 able considering that the dipole sources generating the MRCP are primarily
 148 affected by the physical properties of the skull and of the measuring system
 149 which are supposed to be time-invariant), we can estimate A by knowing the
 150 instant in which a movement was imagined or executed during a training ses-
 151 sion. A reference signal is then generated, by placing a prototype waveform in
 152 relation to the movement onsets. Specifically, the prototype is a 1 s long wave
 153 starting from 0 and linearly decreasing until the instant of a moving onset; then,
 154 it instantly reaches 0 in the following time sample (notice that different proto-
 155 types with durations in the range 0.5 - 2 seconds have been tested, obtaining
 156 similar results). Examples of time series A including prototypes corresponding
 157 to movement onsets are superimposed to filtered data in Figures 5. Then, the
 158 vector W is calculated by solving the model on the training set and the MRCP
 159 over time (i.e, A) is computed for new unseen EEG recordings based on the
 160 estimated W :

$$\begin{aligned}
 W &= S^{-1} \cdot A \quad (\text{training set}) \\
 A &= S \cdot W \quad (\text{testing set})
 \end{aligned}
 \tag{2}$$

161 Notice that S is not square, so that it cannot be inverted. It was pseudo-
 162 inverted (Moore-Penrose inverse [26]). Replacing S^{-1} with its pseudo-inverse
 163 allows to minimize the square norm of the residual τ , obtaining the solution
 164 with minimum squared error. Notice that this solution is unlikely to feature a
 165 residual $\tau = 0$, but still represents the best linear combination of channels to
 166 map the MRCPs to our prototype (in the least mean squared sense).

167 2.3.2. Whitening Transformation

Applying a transformation to S (matrix collecting the EEG channels in its
 columns) that makes it spherical, i.e., with covariance equal to the identity
 matrix, can ensure that the model satisfies the last two assumptions of OLS
 method (i.e., orthogonality of predictors and sphericity of residuals), improving
 the reliability of the results.

Thus, whitening was employed, by using singular value decomposition (SVD). Consider the factorization of the matrix S written as

$$S = U\Sigma V^T$$

where U and V are orthonormal. The matrix Σ is square diagonal, so that its inversion is immediate and can be used to whiten matrix S

$$S^w = UV^T$$

$$S^{w+} = VU^T$$

where S^w and S^{w+} are the whitened matrix and its pseudo-inverse, respectively.

In summary, the linear model now works as follows. The optimal vector is obtained processing the training signal:

$$W = S^{w+} \cdot A \quad (\text{training set})$$

This vector is used to define the filter to be applied:

$$s_{est}(t) = S_{test}^w \cdot W \quad (\text{testing set})$$

168 where $s_{est}(t)$ is the filtered signal obtained by processing the test data S_{test} ,
 169 which ideally should be equal to the prototype waveform during an MRCP and
 170 zero otherwise.

171 Notice that this method not only emphasizes the signal in the epochs containing
 172 the movements intention, while reducing the amplitude out of those epochs, but
 173 it also forces the MRCPs to be all similar, which could be useful to identify
 174 them.

175 2.3.3. Non-linear method

176 Up until now, the method we devised is only able to infer linear mappings be-
 177 tween the EEG signal and the MRCPs. In the field of machine learning, a
 178 common strategy to allow separation of non-linear data (e.g., in the theory of

179 support vector machines, SVM) is known as the kernel trick [27]. The method
180 is based on the assumption that non linearly separable data can be linearly sep-
181 arated when mapped in a different, usually higher dimensional, feature space
182 [28].

183 The idea of extending the dimensionality of the dataset by a non-linear trans-
184 formation was also applied here. The data, after being extended by a non-linear
185 function, were linearly classified, following the same method detailed in Section
186 2.3.1. The Radial Basis Function (RBF, which is a common kernel) was used
187 to transform our EEG data. It maps the data in an infinite dimensional space
188 and allows a linear classifier to learn any smooth non-linear function [27][28]. In
189 order to reduce the computational cost and memory storage, we approximated
190 the kernel in a finite dimensional feature space [29]. Specifically, the Fourier
191 transform of a RBF $p(\omega)$ is a Gaussian function, which is positive and real (this
192 property holds also for other common shift invariant kernels, by Bochner’s theo-
193 rem [29]). Thus, after normalization, we can consider it as a probability density
194 function (i.e., a positive function with integral equal to 1). Hence, writing the
195 RBF as the inverse transform of $p(\omega)$, we can interpret it as the mean value of
196 the complex exponential, or of the cosine function, as both the kernel and its
197 transform are real. The RBF was then estimated using a set of cosine func-
198 tions with random frequencies with distribution $p(\omega)$ and uniformly distributed
199 phases (see [29] for details). The new kernel has finite dimensionality and can
200 be simply reconstructed from the sampled points, so we can use it to explicitly
201 map the EEG data to a high dimensional space before feeding it to the linear
202 algorithm fitting the MRCPs.

203 In summary, the non-linear mapping is obtained by the following steps.

- 204 • Set a probability distribution $p(\omega)$ as the discrete Fourier transform of
205 the kernel normalized to have unitary integral (notice that our kernel is
206 Gaussian and its Fourier transform is too).
- 207 • Set $\Omega = \{\omega_i\}$ as N vectors of nc elements extracted from the distribution
208 $p(\omega)$ (notice that N is a hyper-parameter to be selected).

209 • Set $B = \{b_i\}$ (random phases) as N samples taken from the uniform
 210 distribution between 0 and 2π .

- Define the i^{th} dimension of the non-linear map as

$$\cos(\omega_i \cdot \mathbf{x} + b_i) \quad (3)$$

211 where \mathbf{x} indicates the EEG data.

212 In this way, N time series are obtained, which are non-linear combinations of
 213 the EEG data. To those data, the linear method (described before) is applied
 214 to fit the prototype MRCP component A .

215 As shown by a fine tuning on preliminary tests using the measurements from
 216 subject 16 (as mentioned above), a dimension $N = 200$ is enough to provide a
 217 significant performance boost to the algorithm without overfitting. The steps
 218 of this innovative non-linear filter are shown in Figure 4.

219 2.4. Comparison with a state-of-the-art method

220 We have reproduced for comparison the Optimized Spatial Filter (OSF), with
 221 quasi-Newton BFGS algorithm [2].

The method calculates a virtual channel as a zero-mean linear combination of the EEG data such as to emphasize the energy of the MRCPs with respect to the noise:

$$\begin{aligned} \text{maximize : } & 10 \cdot \log_{10} \left[\frac{P(\sum_{k=1}^{nc} x_k S_k(t))}{P(\sum_{k=1}^{nc} x_k N_k(t))} \right] \\ \text{subject to : } & \sum_{k=1}^{nc} x_k = 0 \end{aligned}$$

where $P(\cdot)$ indicates power, nc is the number of EEG channels, S the concatenation of signal epochs (in which MRCPs were present) and N the noise (concatenation of epochs in which the MRCP was absent). The windows in which a MRCP is present and absent are taken in the training data set. Starting from the coefficients of the Laplacian spatial filter

$$x_k = \begin{cases} 1, & k = 1 \\ -\frac{1}{nc-1} & k \neq 1 \end{cases} \quad (4)$$

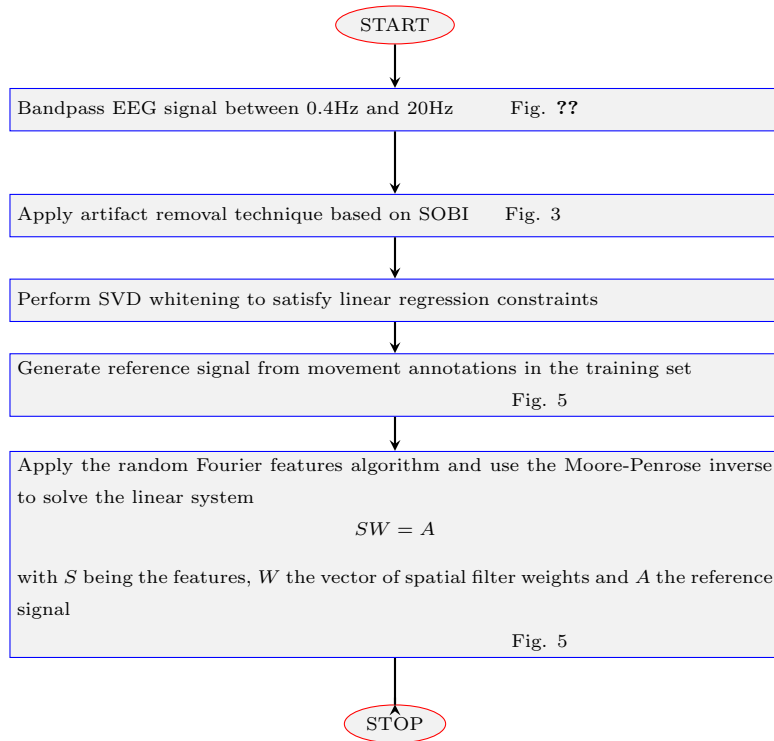


Figure 4: Overview of the NL-SF algorithm in the training phase (during the test, the data are whitened, processed by the random Fourier features algorithm and applied to the vector of spatial filter weights W to estimate the filtered signal).

222 where $k = 1$ for the electrode Cz, the coefficients are updated using the BFGS
 223 algorithm in order to maximize the SNR of such a linear combination.

Here, the constraint that the filter coefficients have zero sum was implicitly parametrized inside the loss function by using a penalty term

$$\text{minimize} : \left(10 \cdot \log_{10} \left[\frac{P(\sum_{k=1}^{nc} x_k S_k(t))}{P(\sum_{k=1}^{nc} x_k N_k(t))} \right] \right)^{-1} + \left(\sum_{k=1}^{nc} x_k \right)^2$$

224 *2.5. Identification of the MRCP and performance metrics*

225 The outputs of the two filters were post-processed in the same way to perform a
 226 classification task, i.e., discriminating between windows that include an MRCP
 227 or not. Specifically, a lowpass exponential filter of order 2 was first used. Then,

228 a template was obtained by averaging aligned MRCPs extracted from the train-
229 ing set. This template was used to build a match filter, with optimal threshold
230 computed based on the Receiver Operating Characteristics curve applied on the
231 training data. Then, it was applied on test data and the results were computed
232 on 2 s segmented windows of EEG. For every movement intention of the user
233 (thus, either executed or imagined movement), a single window is taken con-
234 taining the 2 s before it and a second window is taken from 4 to 6 s before it,
235 in an interval in which there are no MRCPs. The algorithms are then asked to
236 solve a balanced classification problem.

237 The metrics chosen for the evaluation of the performances are the Accuracy,
238 the True Positive Rate (TPR) and the False Positive Rate (FPR). They have
239 been reported per-participant alongside the global mean and standard deviation.
240 Performances of the two methods were compared using Wilcoxon signed rank
241 test.

242 Some tests have also been made by changing some parameters from the default
243 conditions. Specifically, the effect of reducing the number of detection channels
244 was tested, by measuring classification performances when using a lower num-
245 ber of channels: the electrodes F3, P4 and Fz have been removed. Moreover,
246 the effect of reducing the training data was investigated: instead of using the
247 training set including the 70% of the data, performances were also computed
248 reducing the training to the 40% of the MRCPs. The Wilcoxon signed rank
249 test was applied to make specific paired comparisons of the performances of the
250 methods when either the number of recording channels or the training set were
251 reduced.

252 **3. Results**

253 The output of the two filters OSF and NL-SF is shown in Figure 5 for a few
254 representative data (i.e., from the first 3 participants, during the motor exe-
255 cution task). Notice that NL-SF shows waveforms corresponding to movement
256 onsets which are more similar among them, with respect to those obtained by

257 the OSF. The mean and standard error of MRCPs (aligned and averaged on
 258 the basis of the instants of movement onsets) are shown in Figure 6 for the two
 259 filters, considering the same data of the previous figures. Notice that the aver-
 260 age MRCPs obtained by the NL-SF show smaller oscillations (with an almost
 261 monotonic decrease) than those provided by the OSF. The variabilities of the
 262 MRCPs identified by the two filters were quantified as the average over time of
 263 the standard error (across epochs) divided by the mean of the absolute value of
 264 the average MRCP: their mean \pm std were 0.35 ± 0.15 and 0.16 ± 0.03 , for the OSF
 265 and the NL-SF, respectively; Wilcoxon signed rank test indicated a statistically
 266 significant difference, with $p=0.002$.

267 The performances of the two methods on every participant are reported in Tables
 268 1 and 2, considering TPR and FPR (respectively), either in motor execution or
 269 imagination.

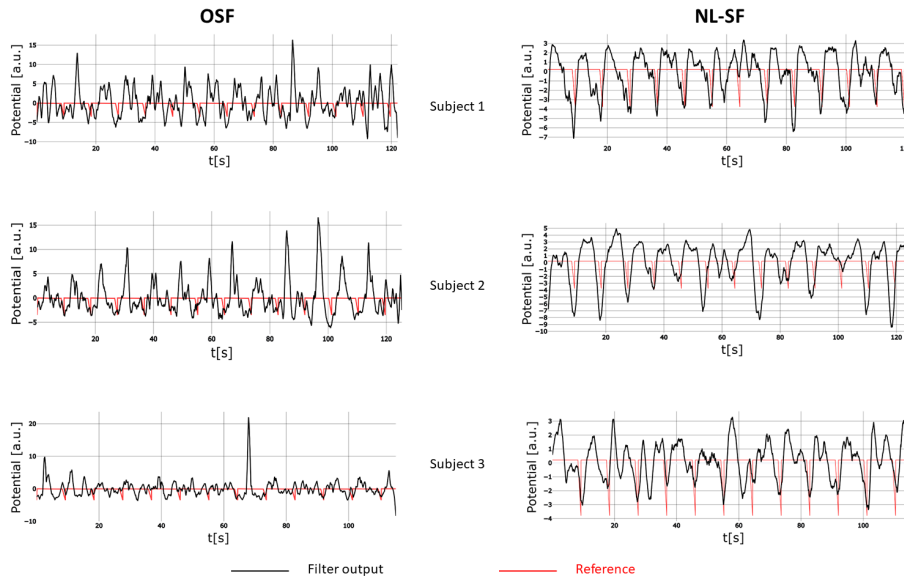


Figure 5: Representative filtered data obtained by the OSF (left) and the NL-SF (right) superimposed to the prototype (indicating movement onset at the peak of the triangular waveforms), during motor execution.

270 Performance indexes show some statistically significant variation among the two

True Positive Rate				
Participant ID	Motor Execution		Motor Imagination	
	OSF	NL-SF	OSF	NL-SF
1	0.54	0.92	1.00	0.83
2	1.00	0.77	0.92	0.92
3	0.67	0.67	0.83	0.67
4	0.67	0.83	0.38	0.62
5	0.77	0.85	0.69	0.77
6	0.77	0.85	0.75	0.92
7	1.00	1.00	0.58	0.83
8	0.85	0.38	0.38	0.69
9	0.92	0.83	0.50	0.83
10	0.57	0.71	0.92	0.69
11	0.62	0.69	0.62	0.85
12	0.69	0.85	0.23	0.85
13	0.54	0.92	0.92	0.92
14	0.92	0.92	0.69	0.85
15	0.75	0.75	0.69	0.92
16			1.00	0.92

Table 1: True Positive Rate of methods based on optimal spatial filter (OSF) and non-linear optimal spatial filter (NL-SF) applied to test EEG data (last 30% of our recordings) acquired during either Motor Execution or Imagination (subject number 16 during motor execution is excluded, as the data were used for hyper-parameter optimization).

False Positive Rate				
Participant ID	Motor Execution		Motor Imagination	
	OSF	NL-SF	OSF	NL-SF
1	0.15	0.38	0.00	0.00
2	0.00	0.07	0.08	0.00
3	0.25	0.17	0.42	0.33
4	0.33	0.08	0.46	0.46
5	0.00	0.23	0.15	0.23
6	0.00	0.00	0.17	0.17
7	0.00	0.00	0.25	0.25
8	0.23	0.08	0.15	0.23
9	0.25	0.25	0.00	0.25
10	0.00	0.00	0.08	0.31
11	0.31	0.31	0.15	0.08
12	0.54	0.15	0.15	0.00
13	0.00	0.23	0.08	0.17
14	0.15	0.00	0.31	0.15
15	0.17	0.08	0.38	0.23
16			0.00	0.00

Table 2: False Positive Rate of methods based on optimal spatial filter (OSF) and non-linear optimal spatial filter (NL-SF) applied to EEG data acquired during either Motor Execution or Imagination.

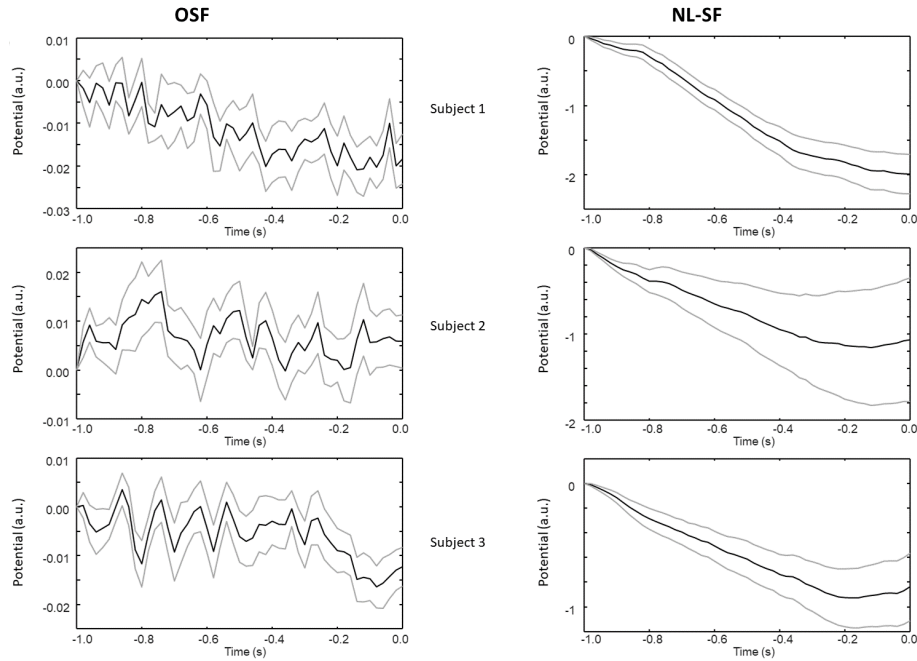


Figure 6: Mean and Standard Error of MRCPs in the testing set of 3 subjects, obtained by the OSF (left) and the NL-SF (right).

271 methods. The median accuracy was always larger for the NL-SF than for the
 272 OSF (see Figure 7), but the sample number was small and statistical significance
 273 was not disclosed in the motor execution and motor imagination groups. The
 274 post-hoc test shows that in motor imagination the true positive rate of NL-SF
 275 is better ($p < 0.05$) than for the OSF. Pooling together motor execution and
 276 imagination (thus increasing the sample number), the NL-SF is superior than
 277 OSF in terms of accuracy ($p = 0.04$, median accuracy of 76.9% and 84.6%, for
 278 the OSF and NL-SF, respectively) and true positive rate ($p = 0.04$, median TPR
 279 of 69.2% and 83.3%, for the OSF and NL-SF, respectively).

280 The effect of a reduction of either the number of EEG channels or the size of
 281 the training set is shown in Figure 7. Considering the overall dataset (including
 282 motor execution and imagination), the accuracy obtained using the NL-SF is
 283 statistically greater than OSF when decreasing the number of channels (me-

284 dian accuracy 75.0% for OSF, 84.6% for NL-SF, $p=0.035$). Moreover, possible
285 differences in performances when considering motor execution or imagination
286 are tested (paired test, removing from the motor imagination the participant
287 whose data during motor execution were used for hyper-parameter optimiza-
288 tion). Notice that performances decrease only in a few conditions, showing that
289 the methods are quite stable to problems or to a reduction of information in the
290 data (either due to motor imagination instead of execution or to a reduction of
291 channels or training examples).

292 **4. Discussion**

293 A method for extracting the MRCP component from EEG recordings has been
294 developed and tested on 15 recordings from different healthy subjects performing
295 self-paced hand movements and 16 recordings of the same subjects imagining
296 to perform such hand movements. Our approach is based on a non-linear filter,
297 mapping multi-channel EEG into a filtered signal. This signal should be ideally
298 zero except when the user either performs or imagines a movement, in which
299 case a prototype similar to an MRCP emerges.

300 In the tests, the performances of our method overcome those of another filter,
301 i.e., the OSF [2]. The main focus of the OSF is in increasing the energy of
302 the potential in the epochs in which the MRCP is present and decreasing it
303 when it is absent. However, the filter responses during different MRCPs are
304 not constrained to be similar. On the other hand, our filter forces both that
305 the output is large only when the MRCP is present and that it is similar for
306 different MRCPs. The result is that the output of our filter is much more
307 consistent during motor intention of the participants than that of the OSF
308 (Figures 5).

309 It is worth noticing that the OSF presented here was coupled with pre-processing
310 techniques which are adapted to our data and to the need of assessing the perfor-
311 mance in realistic online conditions (in which subjective removal of perturbed
312 epochs cannot be applied). Thus, the pre-processing was different from that

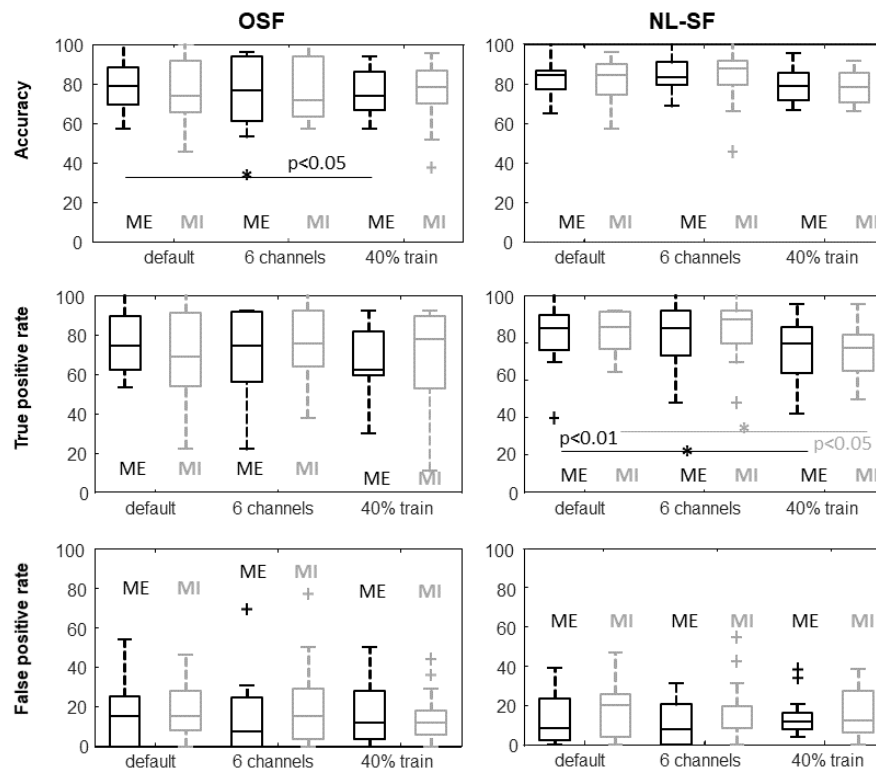


Figure 7: Performances of the filters on the testing set as a function of the experimental modality (either motor execution or imagination) and the reduction of either the number of channels (6 instead of the 9 channels of the default model) or the size of the training set (40% of the MRCs instead of the 70% of the default model). Box and whiskers plots are shown, indicating median, quartiles, range and outliers (using + markers). Statistical differences in paired comparisons ($p < 0.01$) are shown with marker * and a segment joining the two tested distributions.

313 used in the original paper in which it was proposed, where the blink was not
 314 attenuated automatically by a filter, but epochs with a clear blink were removed
 315 [2].

316 Consider also that the techniques we employed to pre-process the signal could be
 317 not optimal in other applications or they could have poor generalization. Indeed,
 318 the literature in the field of EEG processing and multivariate signal analysis

319 presents many interesting techniques which could be tested as preliminary step
320 (e.g., to remove artifacts or reduce noise) to select the optimal combination of
321 pre-processing for the specific application.

322 In summary, our technique is based on a filter that provides better performances
323 than OSF in identifying the MRCP (when they are post-processed by the same
324 method, based on template matching). Even being aware of the still limited ac-
325 curacy and inter-subject variability, we expect that there is room for improving
326 performances of our method as the patient learns and adapts to the BCI during
327 self-paced sessions [11]. Results hold up with a low number of channels as well
328 as in the case of a reduced training set, as shown in Figure 7.

329 **5. Conclusions**

330 An innovative non-linear EEG filter has been developed for identification of
331 MRCP during motor execution or imagination. The results are promising,
332 showing better performances than a previous state-of-the-art filter. Thus, our
333 algorithm could be of interest for application in self-paced BCI.

334 **Appendix - OLS Assumptions**

335 The main OLS assumptions are discussed.

336 *The residuals should have zero conditional mean.* This is also known as the
337 exogeneity constraint. The main causes of failure of exogeneity are the following
338 [30]:

- 339 • Measurement error;
- 340 • Reverse causality;
- 341 • Omitted variables;
- 342 • Omitted sample selection;
- 343 • Lagged dependent variables.

344 We can easily see that our predictor matrix S should not be affected by these
345 items (under proper measurement conditions and provided that the process
346 which maps the source of the MRCPs to each channel does not affect its
347 phase).

348 *The predictors should be linearly independent.* There is no guarantee that this
349 assumption is verified. In fact, different channels could record the activity of the
350 same sources in the brain or of different sources which have correlated activity.
351 Whitening the data imposes this hypothesis to hold.

352 *The residuals should be spherical.* This implies that the variance of the residual
353 is diagonal and not dependent on time. If we assume that the MRCPs are small
354 compared to the matrix S and thus the EEG signal, we can ensure that this
355 assumption is close to be verified, by imposing the matrix S to be spherical
356 itself.

357 **Acknowledgments**

358 Competing interests: None declared

359 Funding: None

360 Ethical approval: All subjects participating to the recordings gave their written
361 informed consent and procedures were approved by the local ethical committee
362 (number 20130081).

363 **References**

- 364 [1] A. Shakeel, M. Navid, M. Anwar, S. Mazhar, M. Jochumsen, I. Ni-
365 azi, A review of techniques for detection of movement intention using
366 movement-related cortical potentials, *Comput Math Methods Med.* 2015
367 (2015) 346217. doi:10.1155/2015/346217.
- 368 [2] I. Niazi, N. Jiang, O. Tiberghien, J. Nielsen, K. Dremstrup, D. Farina, De-
369 tection of movement intention from single-trial movement-related cortical
370 potentials, *J. Neural Eng.* 8 (6) (2011) 066009.

- 371 [3] L. van Dokkum, T. Ward, I. Laffont, Brain computer interfaces for neu-
372 rorehabilitation – its current status as a rehabilitation strategy post-
373 stroke, *Annals of Physical and Rehabilitation Medicine* 58 (1) (2015) 3–8.
374 doi:10.1016/j.rehab.2014.09.016.
- 375 [4] E. Leuthardt, G. Schalk, J. Roland, A. Rouse, D. Moran, Evolution of
376 brain-computer interfaces: going beyond classic motor physiology, *Neuro-
377 surg Focus*. 27 (1) (2009) E4. doi:10.3171/2009.4.FOCUS0979.
- 378 [5] J. Vidal, Toward direct brain-computer communication, *Annual Review of
379 Biophysics and Bioengineering* 2 (1) (1973) 157.
- 380 [6] C. Guger, R. Spataro, B. Allison, A. Heilinger, R. Ortner, W. Cho,
381 V. La Bella, Complete locked-in and locked-in patients: Command fol-
382 lowing assessment and communication with vibro-tactile p300 and motor
383 imagery brain-computer interface tools, *Front. Neurosci.* 11 (2017) 251.
384 doi:10.3389/fnins.2017.00251.
- 385 [7] Y. Shahriari, T. Vaughan, L. McCane, B. Allison, J. Wolpaw, D. Krusien-
386 ski, An exploration of bci performance variations in people with amy-
387 otrophic lateral sclerosis using longitudinal eeg data, *J. Neural Eng.* 16 (5)
388 (2019) 056031. doi:10.1088/1741-2552/ab22ea.
- 389 [8] R. Alcaide-Aguirre, S. Warschausky, A. Brown, D. Aref, J. Huggins,
390 Asynchronous brain-computer interface for cognitive assessment in peo-
391 ple with cerebral palsy, *J Neural Eng.* 14 (6) (2017) 066001. doi:
392 10.1088/1741-2552/aa7fc4.
- 393 [9] E. Holz, L. Botrel, T. Kaufmann, A. Kubler, Long-term independent brain-
394 computer interface home use improves quality of life of a patient in the
395 locked-in state: a case study, *Arch Phys Med Rehabil.* 96 ((3 Suppl)) (2015)
396 S16–26. doi:10.1016/j.apmr.2014.03.035.
- 397 [10] A. Ramos-Murguialday, M. Schurholz, V. Caggiano, M. Wildgruber,
398 A. Caria, E. Hammer, S. Halder, N. Birbaumer, Proprioceptive feedback

- 399 and brain computer interface (bci) based neuroprostheses, PLoS One 7 (10)
400 (2012) e47048. doi:10.1371/journal.pone.0047048.
- 401 [11] M. Grosse-Wentrup, D. Mattia, K. Oweiss, Using brain-computer interfaces
402 to induce neural plasticity and restore function., J. Neural Eng. 8 (2011)
403 025004. doi:10.1088/1741-2560/8/2/025004.
- 404 [12] M. L.M., S. Heckman, D. McFarland, G. Townsend, J. Mak, E. Sellers,
405 D. Zeitlin, L. Tenteromano, J. Wolpaw, T. Vaughan, P300-based brain-
406 computer interface (bci) event-related potentials (erps): People with amy-
407 trophic lateral sclerosis (als) vs. age-matched controls., Clin Neurophysiol.
408 126 (11) (2015) 2124–2131. doi:10.1016/j.clinph.2015.01.013.
- 409 [13] S. Ajami, A. Mahnam, V. Abootalebi, Development of a practical high
410 frequency brain-computer interface based on steady-state visual evoked
411 potentials using a single channel of eeg., Biocybernetics and Biomedical
412 Engineering 38 (1) (2018) 106–114. doi:10.1016/j.bbe.2017.10.004.
- 413 [14] G. Birch, Z. Bozorgzadeh, S. Mason, Initial on-line evaluations of the lfasd
414 brain-computer interface with able-bodied and spinal-cord subjects using
415 imagined voluntary motor potentials., IEEE Trans Neural Sys Rehab Eng.
416 10 (4) (2002) 219–224. doi:10.1109/TNSRE.2002.806839.
- 417 [15] R. Xu, N. Jiang, A. Vuckovic, M. Hasan, N. Mrachacz-Kersting, D. Al-
418 lan, M. Fraser, B. Nasserolelami, B. Conway, K. Dremstrup, D. Farina,
419 Movement-related cortical potentials in paraplegic patients: abnormal pat-
420 terns and considerations for bci-rehabilitation, Front. Neuroeng. 7 (2014)
421 35. doi:10.3389/fneng.2014.00035.
- 422 [16] A. Schwarz, M. Holler, J. Pereira, P. Ofner, G. Muller-Putz, Decoding hand
423 movements from human eeg to control a robotic arm in a simulation envi-
424 ronment, J Neural Eng. 17 (3) (2020) 036010. doi:10.1088/1741-2552/
425 ab882e.

- 426 [17] Y. Gu, D. Farina, A. Ramos-Murguialday, K. Dremstrup, N. Birbaumer,
427 Comparison of movement related cortical potential in healthy people and
428 amyotrophic lateral sclerosis patients, *Front. Neurosci.* 7 (2013) 65.
- 429 [18] N. Jiang, N. Mrachacz-Kersting, R. Xu, K. Dremstrup, D. Farina,
430 An accurate, versatile, and robust brain switch for neurorehabilitation,
431 Guger, Christoph & Vaughan, Theresa & Allison, Brendan. (2013). *Brain-*
432 *Computer Interface Research: A State-of-the-Art Summary* 3 (2013) 58.
433 doi:10.1007/978-3-319-09979-8.
- 434 [19] C. Jeunet, E. Jahanpour, F. Lotte, Why standard brain-computer inter-
435 face (bci) training protocols should be changed: an experimental study., *J.*
436 *Neural Eng.* 13 (3) (2016) 036024. doi:10.1088/1741-2560/13/3/036024.
- 437 [20] K. Dremstrup, I. Niazi, M. Jochumsen, N. Jiang, D. Mrachacz-Kersting,
438 N. Farina, Rehabilitation using a brain computer interface based on move-
439 ment related cortical potentials. a review, XIII Mediterranean Conference
440 on Medical and Biological Engineering and Computing 2013. Ed. by Laura
441 M. Roa Romero. Cham: Springer International Publishing (2014) 1659–
442 1662.
- 443 [21] R. Scherer, J. Faller, P. Sajda, C. Vidaurre, Eeg-based endogenous on-
444 line co-adaptive brain-computer interfaces: Strategy for success?, 10th
445 Computer Science and Electronic Engineering (CEECE), Colchester, United
446 Kingdom (2018) 299–304doi:10.1109/CEECE.2018.8674198.
- 447 [22] F. Karimi, J. Kofman, N. Mrachacz-Kersting, D. Farina, N. Jiang, Detec-
448 tion of movement related cortical potentials from eeg using constrained ica
449 for brain-computer interface applications, *Front. Neurosci.* 11 (2017) 356.
450 doi:10.3389/fnins.2017.00356.
- 451 [23] L. De Lathauwer, J. Castaing, Second-order blind identification of underde-
452 termined mixtures. independent component analysis and blind signal sepa-
453 ration, Ed. by Justinian Rosca, Deniz Erdogmus, José C. Príncipe, Simon
454 Haykin. Berlin, Heidelberg: Springer Berlin Heidelberg (2006) 40–47.

- 455 [24] G. Gomez-Herrero, W. Clercq, H. Anwar, K. Kara, O. Egiazarian, S. Huffel,
456 W. Paesschen, Automatic removal of ocular artifacts in the eeg without an
457 eeg reference channel., Proceedings of the 7th Nordic Signal Processing
458 Symposium (2006) 130–133.
- 459 [25] C. Sevcik, A procedure to estimate the fractal dimension of waveforms,
460 Complexity International 5 (2018).
- 461 [26] C. Rao, S. Mitra, Generalized inverse of matrices and its applications, New
462 York: John Wiley & Sons. (1971).
- 463 [27] T. Hofmann, B. Scholkopf, A. Smola, Kernel methods in machine
464 learning, The Annals of Statistics 36 (3) (2008) 1171–1220. doi:10.
465 121400905360700000677.
- 466 [28] S. Theodoridis, K. Koutroumbas, Pattern recognition, Academic Press
467 (2008).
- 468 [29] A. Rahimi, B. Recht, Random features for large-scale kernel machines,
469 Advances in Neural Information Processing Systems 20. Ed. by J. C. Platt,
470 Daphne Koller, Yoram Singer, Sam T. Roweis, Curran Associates, Inc.
471 (2008) 1177–1184.
- 472 [30] N. Uttam Singh, K. Das, A. Roy, How to test endogeneity or exogeneity:
473 an e-learning hands on sas.